

ENHANCEMENT OF CHARM QUARK PRODUCTION DUE TO NONLINEAR CORRECTIONS TO THE DGLAP EQUATIONS

K.J. Eskola^{a,b1}, V.J. Kolhinen^{a2} and R. Vogt^{a,c3}

^a*Department of Physics, University of Jyväskylä,
P.O. Box 35, FIN-40014 University of Jyväskylä*

^b*Helsinki Institute of Physics,
P.O. Box 64, FIN-00014 University of Helsinki, Finland*

^c*Lawrence Berkeley National Laboratory, Berkeley, CA 94720, USA,
and
Physics Department, University of California, Davis, CA 95616, USA*

Abstract

We have studied how parton distributions based on the inclusion of nonlinear scale evolution and constraints from HERA data affect charm production in pp collisions at center-of-mass energies of 5.5, 8.8 and 14 TeV. We find that, while the resulting enhancement can be substantial, it is very sensitive to the charm quark mass and the scale entering the parton densities and the strong coupling constant.

¹kari.eskola@phys.jyu.fi

²vesa.kolhinen@phys.jyu.fi

³vogt@lbl.gov

1 Introduction

Global fits of the parton distribution functions (PDFs) such as those by CTEQ [1, 2] and MRST [3, 4, 5], based on the Dokshitzer-Gribov-Lipatov-Altarelli-Parisi (DGLAP) [6] scale evolution, successfully describe the proton structure function, $F_2(x, Q^2)$, deep inelastic scattering (DIS) data in the “high (Q^2, x) ” region, $Q^2 \gtrsim 10 \text{ GeV}^2$ and $x \gtrsim 0.005$. However, it is not possible to maintain the excellent high (Q^2, x) DIS fit while simultaneously fitting the “low (Q^2, x) ” region, $1.5 \lesssim Q^2 \lesssim 10 \text{ GeV}^2$ and $x \lesssim 0.005$ [5]. In addition, the next-to-leading order (NLO) gluon distribution becomes negative for sufficiently small x at the few GeV^2 scales.

Nonlinear corrections to the PDF evolution based on gluon recombination were first derived by Gribov, Levin and Ryskin [7] as well as Mueller and Qiu [8]. Recent work [9] showed that adding these GLRMMQ terms to the DGLAP equations can improve the overall leading order (LO) fits to the HERA DIS data [10]. The rapid Q^2 evolution in the low (Q^2, x) region from DGLAP alone is slowed by the GLRMMQ recombinations. At Q^2 scales far above the initial scale Q_0^2 , the Q^2 evolution of the PDFs is again described by the DGLAP equations since the GLRMMQ terms become negligible, see Fig. 1.

While the quark distributions are directly constrained by the HERA $F_2(x, Q^2)$ data, the gluon distribution is constrained by the F_2 slope, $\partial F_2 / \partial \ln Q^2$. The fairly modest measured slopes force the LO DGLAP gluon distributions to be nearly independent of x for scales of a few GeV^2 [1, 3] and also force the NLO gluons to be negative. When the nonlinear terms are included, the slowing of the Q^2 evolution leads to an enhancement of the small- x gluon distributions at $Q^2 \lesssim 10 \text{ GeV}^2$ relative to the LO DGLAP gluon distributions, subject to the same constraints from HERA [9]. The effect of nonlinear evolution on the NLO distributions is not yet fully explored by global fits which include the low (Q^2, x) region but the results of Ref. [5] suggest that the enhancement is smaller than at LO. This effect alone thus seems unlikely to produce positive NLO small x gluon distributions at the few GeV^2 scales.

In spite of the problems described above, the quality of the global DGLAP fits to the HERA data [1, 3] is good. The χ^2 per degree of freedom is close to one even when the low (Q^2, x) region is included. Therefore, F_2 measurements at HERA alone may not clearly differentiate DGLAP from nonlinear evolution and more direct probes of the gluon distribution are needed. In this paper, we study whether the parton distribution functions generated with the LO DGLAP+GLRMMQ evolution in Ref. [9] could give rise to any significant enhancement relative to the DGLAP-evolved PDFs in charm quark hadroproduction. Charm production is the best candidate process since the charm quark mass is relatively low, $1.2 \lesssim m_c \lesssim 1.8 \text{ GeV}$, and its production is dominated by gluons. These two characteristics should lead to the most favorable conditions for a possible effect. The Q^2 scale at which the total cross sections are calculated is proportional to m_c^2 and $4m_c^2$. Thus the results are sensitive to Q^2 . Unfortunately, due to the small charm mass, the scale dependence is still significant at NLO [11].

We focus on pp collisions since these nonlinear distributions are not yet available for

nuclei. Our calculations are at leading order only since the nonlinear parton distribution functions, referred to as EHKQS hereafter, are only evolved to LO in Ref. [9]. We calculate the possible effect as a function of rapidity and transverse momentum of the charm quark and the $c\bar{c}$ pair invariant mass. We study collisions at center-of-mass energies $\sqrt{S} = 5.5, 8.8$ and 14 TeV at the Large Hadron Collider (LHC). These energies correspond to the planned per nucleon energies of Pb+Pb, p Pb and pp collisions, effectively spanning the LHC energy regime.

2 Formalism and inputs

2.1 Cross sections and parton distribution functions

Inclusive differential charm cross sections at high energies are, to first approximation, computable assuming factorization. The cross section may be expressed as

$$d\sigma_{pp \rightarrow c\bar{c}X}(Q^2, \sqrt{S}) = \sum_{i,j,k=q,\bar{q},g} f_i(x_1, Q^2) \otimes f_j(x_2, Q^2) \otimes d\hat{\sigma}_{ij \rightarrow c\bar{c}k}(Q^2, x_1, x_2) \quad (1)$$

where $\hat{\sigma}_{ij \rightarrow c\bar{c}k}(Q^2, x_1, x_2)$ are the perturbatively calculable partonic cross sections for charm production at scales $Q^2 \gg \Lambda_{\text{QCD}}^2$, x_1 and x_2 are the momentum fractions of the partons involved in the hard scattering and $f_i(x, Q^2)$ are the free proton parton densities. At LO, only the gg and $q\bar{q}$ channels are available and $k = 0$, *i.e.* no other partons are produced with the $c\bar{c}$. The LO matrix elements and partonic cross sections for charm production can be found in Ref. [12]. In the following, we consider the triple differential distributions, $d^3\sigma/(dp_T dy dy_2)$, where y and y_2 are the rapidities of the quark and antiquark and p_T is the quark transverse momentum. We also study the inclusive distributions $d\sigma/dy$, $d\sigma/dp_T$ and $d\sigma/dM$ where $M^2 = 2m_T^2(1 + \cosh(y - y_2))$ is the square of the pair invariant mass and $m_T^2 = p_T^2 + m_c^2$ is the transverse mass of the quark.

The new inputs in this straightforward calculation are the nonlinearly-evolved proton PDFs. The EHKQS sets⁴ in Ref. [9] employ the CTEQ5L [13] and CTEQ6L [1] PDFs as a baseline and require a good fit to the HERA $F_2^p(x, Q^2)$ data over the full (Q^2, x) range [9]. Three EHKQS sets were obtained when the GLRMMQ terms were included in the analysis. All three EHKQS sets employ the initial scale $Q_0^2 = 1.4$ GeV² and $\Lambda_{\text{QCD}} = 0.192$ GeV for four flavors but differ in the treatment of the charm mass threshold in the evolution. In set 1, a nonzero charm distribution was allowed at Q_0^2 . Sets 2a and 2b assumed that there was no charm quark distribution below Q_0^2 , turning on when $Q^2 = m_c^2 \geq Q_0^2$. Set 2a assumed $m_c = 1.3$ GeV while set 2b took $m_c = Q_0 = \sqrt{1.4}$ GeV. The input gluon distribution is the same in all cases so that the small differences at high Q^2 arise from the treatment of the charm quark evolution. The choice of set 1, set 2a or set 2b therefore makes very little difference in the overall effect of the nonlinear terms on charm production. Thus we only use EHKQS set 1.

⁴available at www.urhic.phys.jyu.fi

We work at leading order since the EHKQS sets are only evolved to LO using a one-loop evaluation of the strong coupling constant α_s . Thus these LO distributions should generally not be mixed with NLO matrix elements and the two-loop α_s . The charm quark p_T distribution is broadened at NLO relative to the LO calculation [11]. Therefore we study the ratios of calculations with EHKQS relative to those with a standard LO PDF set evolved using the DGLAP equations alone. We quantify the effect with respect to the CTEQ61L parameterization, the most recent LO fit to the PDFs that also uses a one-loop α_s [2]. The minimum scale of CTEQ61L is $Q_0^2 = 1.69 \text{ GeV}^2$. This LO fit obtained a slightly higher value of Λ_{QCD} for four flavors, 0.215 MeV. In our CTEQ61L calculations, for consistency with the PDF set, we use this value in α_s .

2.2 Comparison of EHKQS and CTEQ61L gluon distributions

Before presenting our results, it is instructive to discuss the differences between the EHKQS and CTEQ61L gluon distributions in more detail. Since the high \sqrt{S} collisions studied here probe the very low x region, some remarks on the region of applicability of the PDFs are in order. Below the minimum x and Q^2 values assumed in the fits, the PDFs are essentially unconstrained. At the scales studied here, described in the following section, Q^2 always remains above the minimum scale of the PDF sets. However, the region below the minimum x , x_{\min} , is reached at large rapidities and intermediate scales at the LHC. Thus the behavior of the PDFs below x_{\min} is an uncertainty for all PDFs. This situation can only be improved by more extensive small x constraints on the PDFs.

The minimum x of the EHKQS sets is $x_{\min}^{\text{EHKQS}} = 10^{-5}$. For $x < x_{\min}^{\text{EHKQS}}$ and Q^2 of a few GeV^2 , neglected power-suppressed terms in the evolution become important and the DGLAP+GLRMQ results are no longer trustworthy [9]. The CTEQ61L minimum is an order of magnitude smaller than x_{\min}^{EHKQS} , $x_{\min}^{\text{CTEQ61L}} = 10^{-6}$. The very small x regions below x_{\min} are not excluded from our calculations. Instead, we assume that below x_{\min} , $f_i(x < x_{\min}, Q^2) = f_i(x_{\min}, Q^2)$ for each set. We note that in the CTEQ61L table [14] the distributions are not constant below $x_{\min}^{\text{CTEQ61L}}$.

It is illustrative to compare the EHKQS set 1 and CTEQ61L gluon distributions as a function of Q^2 for several values of x , shown in Fig. 1. Due to the nonlinear evolution, the Q^2 dependence of EHKQS set 1 is rather mild compared to CTEQ61L which approaches a constant at Q_0^2 and $x \rightarrow 0$. Note that for all $x > 10^{-5}$, the EHKQS distributions are always above CTEQ61L although, at higher scales, the distributions lie very close together. In the unconstrained region where $x < 10^{-5}$, the situation clearly depends on how the extrapolation towards $x \rightarrow 0$ is done. The CTEQ61L parameterization continues to $x_{\min}^{\text{CTEQ61L}}$. In this very low x region, at $Q^2 = 4 \text{ GeV}^2$, the CTEQ61L gluon distribution at $x_{\min}^{\text{CTEQ61L}}$ crosses the EHKQS distribution, fixed at the value of x_{\min}^{EHKQS} , and continues to rise. Therefore, the behavior of the relative kinematics distributions we compute can be very sensitive to the treatment of the unconstrained x region. Since the two distributions are also quite sensitive to the

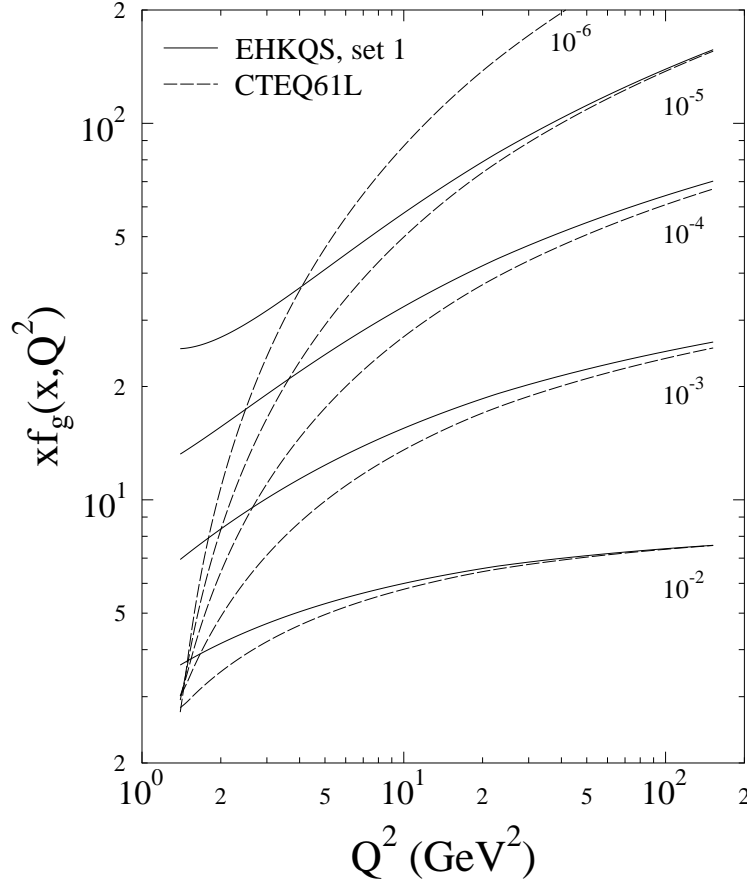


Figure 1: Comparison of the EHKQS set 1 (solid curves) and CTEQ61L (dashed curves) gluon distributions as a function of Q^2 for, from lowest to highest, $x = 10^{-2}$, 10^{-3} , 10^{-4} , 10^{-5} and, for CTEQ61L only, 10^{-6} .

scale, the ratios we compute will also be strongly scale dependent.

2.3 Scale choice

In our calculations, we use values of the charm quark mass and scale that have been fit to the total cross section data using NLO calculations. The total cross section data cannot be fit by adjusting m_c and Q^2 with a full LO calculation, employing LO PDFs and the one-loop α_s , because the resulting m_c would be too small for perturbative applications. See Ref. [11] for more discussion. The best agreement with the total cross section data is obtained with $m_c = 1.2$ GeV and $Q^2 = 4m_c^2$ for standard DGLAP-evolved NLO PDFs such as CTEQ6M [2] and MRST [15]. Nearly equivalent agreement may be obtained with $m_c = 1.3$ GeV and $Q^2 = m_c^2$ [16, 17]. Thus our main results are based on these inputs. Alternative fits to the fixed-target total cross sections can be achieved with larger values of m_c by separating the factorization scale, Q_F , from

the renormalization scale, Q_R , e.g. $Q_F^2 = 4m_c^2$ and $Q_R^2 = m_c^2$ or $m_c^2/4$, and allowing the fast running of α_s in this Q_R^2 region to increase the cross sections. Note that if $Q^2 = Q_F^2 \leq Q_0^2$, the PDFs are unconstrained in Q^2 . We keep $Q_F^2 = Q_R^2$, as in all typical PDF fits such as Refs. [2, 15], limiting ourselves to relatively small values of m_c to obtain agreement with the total cross section data. The PDFs are thus evaluated above Q_0^2 for the masses and scales we use.

Note that we have discussed scales proportional to m_c^2 in the calculations of the total cross sections. Such scales are used because the total NLO partonic cross section can be written analytically as a function of $4m_c^2/s$ where s is the partonic center-of-mass energy squared [18]. In this case, the charm quark mass is the only relevant scale. However, in inclusive distributions such as we compute here, the quark p_T also enters since a scale proportional to m_T^2 is needed to control p_T -dependent logarithms. Therefore, in our calculated ratios of distributions, we take $Q^2 = m_T^2$ with $m_c = 1.3$ GeV and $4m_T^2$ with $m_c = 1.2$ GeV.

Whether the high and low energy behavior of the charm cross section can be described simultaneously by the same values of m_c and Q^2 is an open question. Since the slopes of the gluon distributions differ at low and high x , the scale dependence is a strong function of \sqrt{S} . At high x , $xf_g(x, Q^2)$ is larger at low Q^2 than at higher scales. Thus at fixed target energies, $\sigma(m_c^2) > \sigma(4m_c^2)$. At collider energies, such as at the LHC, x is small and $xf_g(x, Q^2)$ is increasing with Q^2 so that $\sigma(4m_c^2) > \sigma(m_c^2)$ even though $\alpha_s(m_c^2) > \alpha_s(4m_c^2)$. We thus extend the parameter space of our calculations to study the possible effect on higher masses, $m_c = 1.8$ GeV with $Q^2 = m_T^2$ and $4m_T^2$.

3 Results

We start with results insensitive to the unconstrained region at $x < x_{\min} = 10^{-5}$. In inclusive kinematics with an identified charm quark and fixed $x_T = 2m_T/\sqrt{S}$, the unconstrained x -region contributes to charm production at high rapidities, in the region

$$y_u \equiv \ln \left(1/x_T - \sqrt{1/x_T^2 - 1/x_{\min}} \right) \leq |y| \leq \ln \left(1/x_T + \sqrt{1/x_T^2 - 1/x_{\min}} \right) . \quad (2)$$

The upper limit, close to the phase space boundary, is not of interest here. Expanding the lower limit, y_u , in powers of $x_T^2/x_{\min} \ll 1$, we arrive at $y_u \approx \ln[m_T/(x_{\min}\sqrt{S})] \geq \ln[m_c/(x_{\min}\sqrt{S})]$. If $m_c = 1.2$ GeV, the small x region contributes to charm production at $|y| \gtrsim y_u = 2.2, 2.6$ and 3.1 for $\sqrt{S} = 14, 8.8$ and 5.5 TeV, respectively. If $m_c = 1.8$ GeV, the unconstrained region is probed when $|y| \gtrsim y_u = 2.6, 3.0$ and 3.5 , respectively.

First, we study the ratio of the fully differential cross sections calculated with the EHKQS densities relative to the CTEQ61L densities at fixed y and y_2 ,

$$R(p_T, y, y_2) \equiv \frac{d^3\sigma(\text{EHKQS})/(dp_T dy dy_2)}{d^3\sigma(\text{CTEQ61L})/(dp_T dy dy_2)} \quad (3)$$

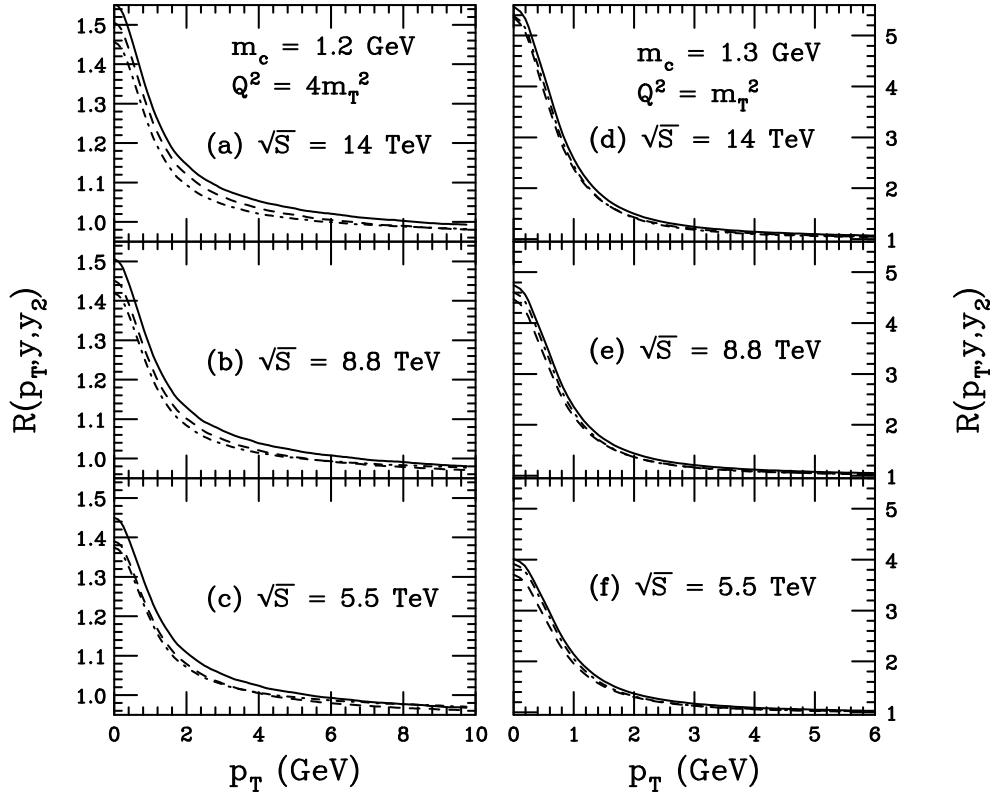


Figure 2: We present $R(p_T, y, y_2)$ for fixed y and y_2 as a function of charm quark p_T at $\sqrt{S} = 14$ TeV, (a) and (d), 8.8 TeV, (b) and (e), and 5.5 TeV, (c) and (f), in pp collisions. The results are shown for $y = y_2 = 0$ (solid curves), $y = 2, y_2 = 0$ (dashed) and $y = y_2 = 2$ (dot-dashed). We show $m_c = 1.2$ GeV and $Q^2 = 4m_T^2$ on the left-hand side and $m_c = 1.3$ GeV and $Q^2 = m_T^2$ on the right-hand side. Note the different scales on the left- and right-hand axes.

In Figs. 2 and 3 we present this unintegrated ratio as a function of p_T for several values of y and y_2 , all within the range constrained by data: $y = y_2 = 0$ (solid curves), $y = 2, y_2 = 0$ (dashed) and $y = y_2 = 2$ (dot-dashed). Figure 2 presents $R(p_T, y, y_2)$ for the values of mass and scale that agree best with the total cross section data, $m_c = 1.2$ GeV and $Q^2 = 4m_T^2$ on the left-hand side and $m_c = 1.3$ GeV, $Q^2 = m_T^2$ on the right-hand side. Figure 3 shows the same unintegrated ratios for our upper limit on m_c , 1.8 GeV and $Q^2 = m_T^2, 4m_T^2$. The center-of-mass energies shown are $\sqrt{S} = 14$ (upper), 8.8 (middle) and 5.5 (lower) TeV.

Figures 2 and 3, which demonstrate the sensitivity of the enhancement to m_c and Q^2 , can be understood by inspection of Fig. 1. At these high energies, the gg channel dominates so that the partonic cross sections essentially drop out of the ratios, and

$$R(p_T, y, y_2) \approx \frac{x_1 f_g(x_1, Q^2)_{\text{EHKQS}}}{x_1 f_g(x_1, Q^2)_{\text{CTEQ61L}}} \frac{x_2 f_g(x_2, Q^2)_{\text{EHKQS}}}{x_2 f_g(x_2, Q^2)_{\text{CTEQ61L}}} \equiv R_g(x_1, Q^2) R_g(x_2, Q^2), \quad (4)$$

where we have denoted the ratio of the EHKQS and CTEQ61L gluons by R_g . The x val-

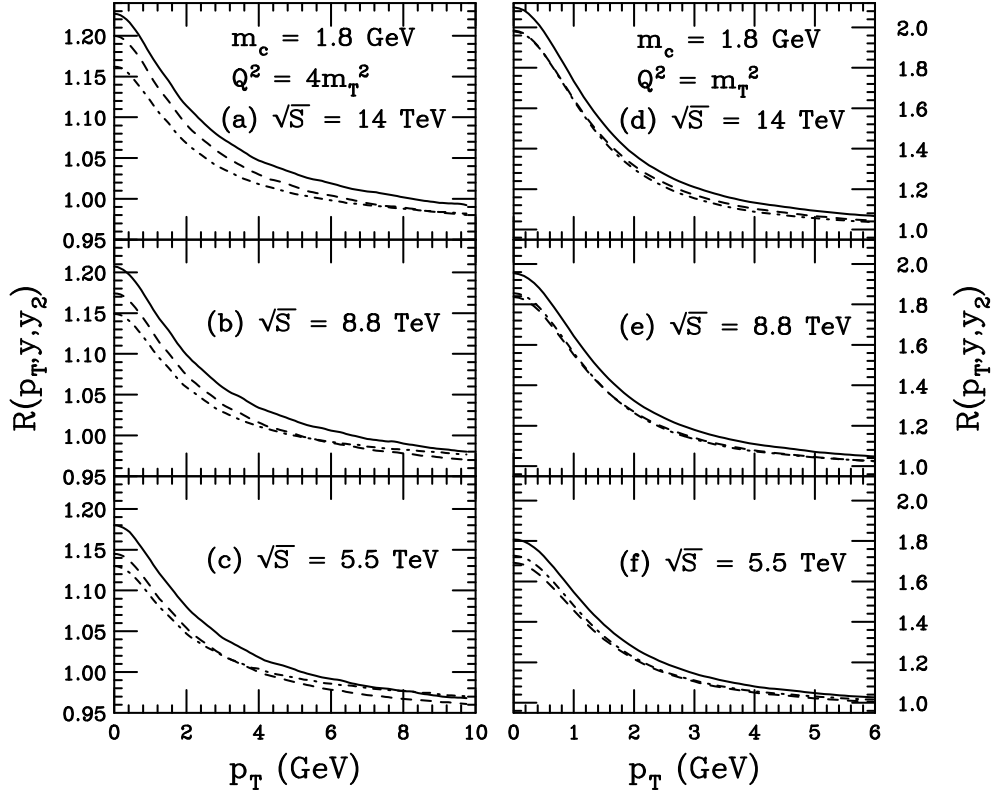


Figure 3: As in Fig. 2 but for $m_c = 1.8$ GeV and $Q^2 = 4m_T^2$ (left-hand side) and for $m_c = 1.8$ GeV and $Q^2 = m_T^2$ (right-hand side). Note the different scales on the left- and right-hand axes.

ues are easily calculated at LO for each curve using the definitions $x_{1,2} = m_T[\exp(\pm y) + \exp(\pm y_2)]/\sqrt{S}$. Since decreasing \sqrt{S} increases x and consequently decreases $R_g(x, Q^2)$, the enhancement decreases with energy. In addition, $R_g(x, Q^2)$ decreases with increasing Q^2 , so that increasing m_c and Q^2 also reduces the enhancement. Both x_1 and x_2 are small when $y = y_2 = 0$ so that the enhancement is largest at midrapidity. Moving away from midrapidity, *e.g.* to $y, y_2 > 0$, increases x_1 and decreases x_2 , correspondingly decreasing $R_g(x_1, Q^2)$ and increasing $R_g(x_2, Q^2)$. The rapidity dependence shown on the right-hand sides of Figs. 2 and 3, for the lower Q^2 , is rather weak. The difference between the dashed ($y = 2, y_2 = 0$) and dot-dashed ($y = y_2 = 2$) curves is very small and the enhancement at $y = y_2 = 2$ lies marginally above that for $y = 2, y_2 = 0$ over all p_T . When the scale is small, the CTEQ61L gluon distribution changes very slowly with x for $x < 0.01$, about 20% for $10^{-4} \leq x \leq 10^{-3}$ when $Q^2 = m_c^2$ and $m_c = 1.3$ GeV ($p_T \approx 0$), so that $R(p_T, y, y_2)$ is not a strong function of y and y_2 . However, the results for the larger scales, shown on the left-hand sides of Figs. 2 and 3, exhibit the opposite behavior along with a stronger rapidity dependence. At larger scales, the slope of the CTEQ61L gluon distribution with x is considerably stronger, resulting in a factor of two difference in the gluon distribution over the range $10^{-4} \leq x \leq 10^{-3}$

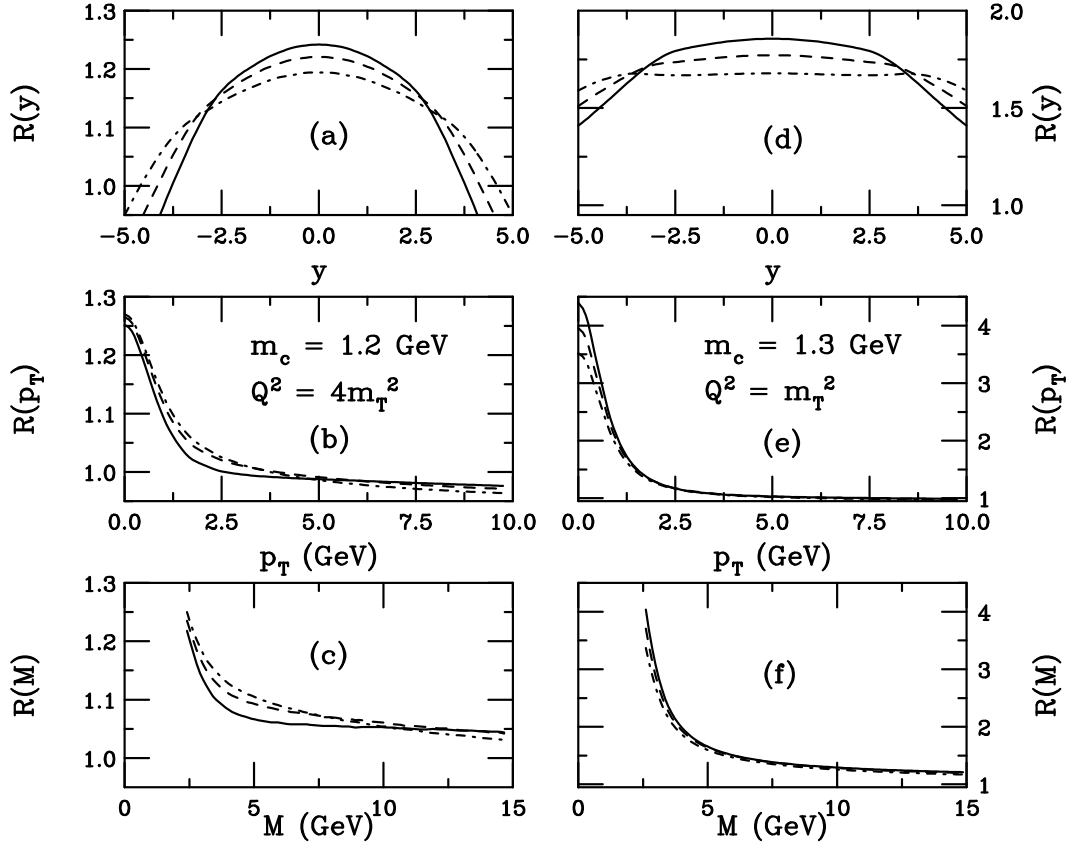


Figure 4: We present $R(y)$, (a) and (d), $R(p_T)$, (b) and (e), and $R(M)$, (c) and (f), in pp collisions at $\sqrt{S} = 14$ (solid), 8.8 (dashed) and 5.5 (dot-dashed) TeV. The left-hand side shows $m_c = 1.2$ GeV and $Q^2 = 4m_T^2$, the right-hand side $m_c = 1.3$ GeV and $Q^2 = m_T^2$.

when $Q^2 = 4m_c^2$ and $m_c = 1.2$ GeV ($p_T \approx 0$), introducing a stronger rapidity dependence of $R(p_T, y, y_2)$ at higher scales. The nonlinearities die out at large scales since the EHKQS gluons become similar to the CTEQ61L gluons so that the enhancement in $R(p_T, y, y_2)$ disappears at large p_T . The ratio does not become equal to 1 because CTEQ61L and the EHKQS sets are not identical either at high Q^2 or larger x . Note that $\alpha_s^2(\text{EHKQS})/\alpha_s^2(\text{CTEQ61L}) \approx 0.9$, allowing $R(p_T, y, y_2)$ to drop below 1 at high p_T .

Next, we turn to the integrated ratios,

$$R(y) \equiv \frac{d\sigma(\text{EHKQS})/dy}{d\sigma(\text{CTEQ61L})/dy}, \quad R(p_T) \equiv \frac{d\sigma(\text{EHKQS})/dp_T}{d\sigma(\text{CTEQ61L})/dp_T}, \quad R(M) \equiv \frac{d\sigma(\text{EHKQS})/dM}{d\sigma(\text{CTEQ61L})/dM}, \quad (5)$$

shown in Figs. 4 and 5. All three energies, $\sqrt{S} = 14$ (solid), 8.8 (dashed) and 5.5 (dot-dashed) TeV, are shown in each plot. Figure 4 shows the integrated ratios for the mass and scale values that best agree with the total cross section data, $m_c = 1.2$ GeV, $Q^2 = 4m_T^2$ on the left-hand side and $m_c = 1.3$ GeV, $Q^2 = m_T^2$ on the right-hand side. Figure 5 shows the corresponding results for $m_c = 1.8$ GeV with $Q^2 = 4m_T^2$ (left-hand side) and m_T^2 (right-hand side).

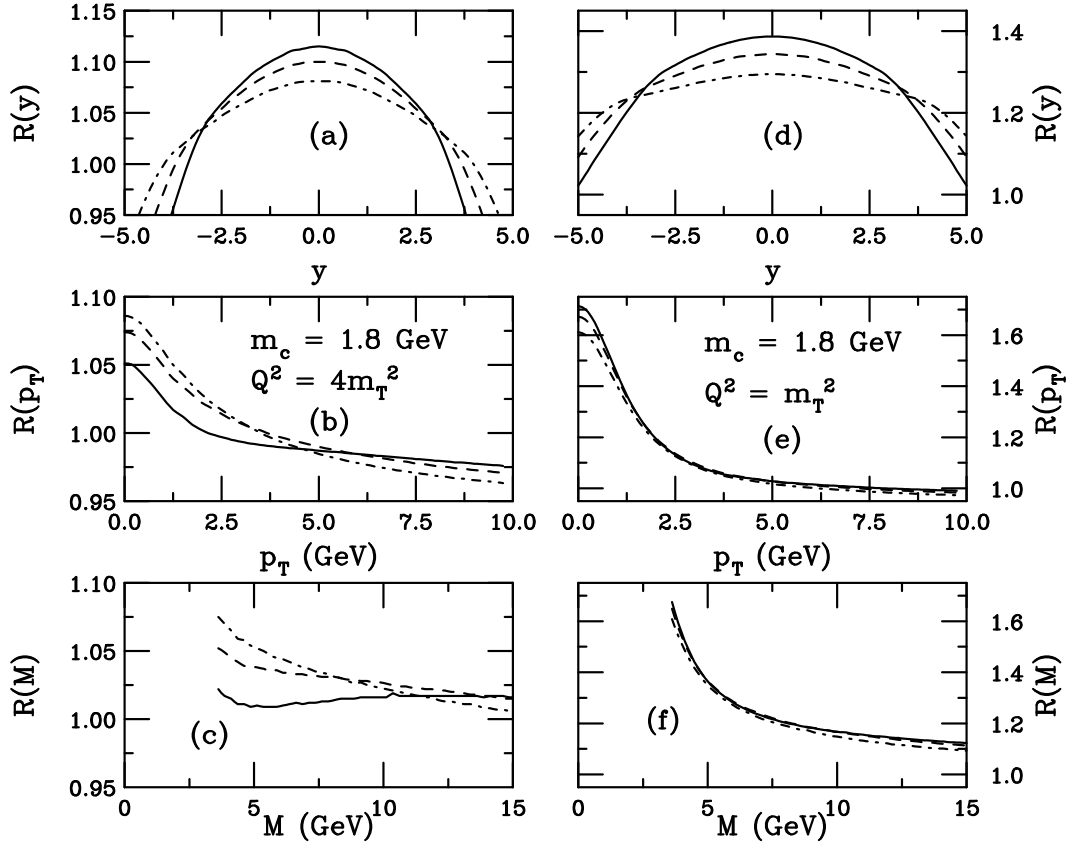


Figure 5: As in Fig. 4 but for $m_c = 1.8$ GeV and $Q^2 = 4m_T^2$ (left-hand side) and $Q^2 = m_T^2$ (right-hand side).

As discussed previously, at midrapidity the results for $R(y)$ are insensitive to the EHKQS extrapolation region $x < x_{\min}^{\text{EHKQS}}$. The magnitude of the enhancement in $R(y)$ can be understood from the unintegrated results. Since $R(y)$ is integrated over p_T , it does not only reflect the enhancement at $m_T = m_c$ ($p_T = 0$) because $Q^2 \propto m_T^2$ [19] and the p_T distribution peaks around $p_T \approx 1$ GeV. When $R(y)$ is calculated with $Q^2 = m_T^2$, shown on the right-hand sides of the figures, the ratios are broad due to the stronger growth of $R_g(x_2, Q^2)$ relative to the reduction of $R_g(x_1, Q^2)$ with increasing y , i.e. decreasing x_2 and increasing x_1 . The ratio is broad because the CTEQ61L gluon distribution is relatively flat as a function of x for $Q^2 \sim 2 - 3$ GeV². The enhancement decreases and broadens with decreasing energy.

The rather sharp turnover in $R(y)$ indicates where the extrapolation region $x < 10^{-5}$ begins to contribute. The rapidity at which $x < 10^{-5}$ is larger for lower energies and larger m_c , see Eq. (2). The clear decrease of $R(y)$ below 1 at large rapidity for $Q^2 = 4m_T^2$ is perhaps surprising. This effect is a consequence of the small- x extrapolation adopted for the PDFs and can be understood through an examination of Fig. 1. While the EHKQS gluon distribution is fixed at its value at $x_{\min}^{\text{EHKQS}} = 10^{-5}$, the CTEQ61L distribution continues to change until $x_{\min}^{\text{CTEQ61L}} = 10^{-6}$. At $\sqrt{S} = 14$ TeV, the rapidity

at which some x values fall below x_{\min}^{EHKQS} is $y_u = 2.2$ (2.6) for $m_c = 1.2$ (1.8) GeV. For $|y| > y_u$ and $Q^2 > 4 \text{ GeV}^2$, as x decreases, the CTEQ61L gluon distribution increases considerably above the EHKQS distribution. Thus $R(y) < 1$ at large rapidities.

Since the rapidity distributions are rather flat, there are still important contributions to the p_T and mass distributions, up to $\sim 30\%$ and 40% respectively at $\sqrt{S} = 14$ TeV for $m_c = 1.2$ and $Q^2 = 4m_c^2$, from the extrapolation region. The contribution from the extrapolation region to $R(M)$ is larger since when m_T^2 is small, M can still be large because the difference $y - y_2$ can be large while either or both y and y_2 can be in the low x region. Thus the sensitivity of $R(p_T)$ and $R(M)$ to the unconstrained region should be kept in mind.

The magnitudes of $R(p_T)$ and $R(M)$ in Figs. 4 and 5 are similar to those of $R(p_T, y, y_2)$ in Figs. 2 and 3. However, the relative energy dependence is reversed from the large to small scales. At the largest \sqrt{S} , the contribution from the $x < 10^{-5}$ region is the largest, and as seen in Fig. 1, if the scales are *e.g.* above 5 GeV^2 , the CTEQ61L gluon density becomes higher than the EHKQS gluon density at $x \leq 10^{-5}$, suppressing $R(p_T)$ relative to $R(p_T, y, y_2)$. At smaller \sqrt{S} the higher x values reduce the contribution to $d\sigma/dp_T$ from the region $x < 10^{-5}$. Thus the suppression of $R(p_T)$ from the extrapolation region is reduced with decreasing energy, explaining the relative values of $R(p_T)$ and $R(M)$ with energy shown with $Q^2 = 4m_T^2$ (the left-hand sides of Figs. 4 and 5). In contrast, for $Q^2 = m_T^2$, the EHKQS gluon density is always higher than CTEQ61L at small x (see Fig. 1), and the energy dependence remains the same as in Figs. 2 and 3.

4 Discussion

Including the GLRMQ terms with DGLAP evolution enhances the low x proton gluon distribution [9]. It may, however, be very difficult to distinguish between linear and nonlinear Q^2 evolution on the basis of the F_2 HERA data alone. Other probes of the low x gluon distribution, such as charm production in DIS at HERA and in pp collisions at the LHC, will hopefully provide the necessary further constraints. In this paper, we have demonstrated how the nonlinear PDFs *constrained by the HERA data* can cause a significant enhancement in the LO charm quark cross sections in pp collisions at the LHC. The enhancement is defined relative to the results expected with the pure DGLAP PDFs which also fit the same HERA data. Quantitatively, however, this enhancement is shown to be very sensitive to the charm quark mass and the scale. Clearly, in addition to collecting more data, further theoretical input, such as high energy resummation of the heavy quark cross sections [20], is needed to reduce this sensitivity.

Our basic message is the following. Currently the high-precision HERA data on the structure function $F_2(x, Q^2)$ and its derivative with respect to Q^2 provide quite stringent constraints on the gluon distribution. Consequently, the CTEQ61L and MRST2001LO gluon distributions are very similar. If a significant enhancement of

charm production, unexpected from DGLAP evolution alone, is found at the LHC, such an enhancement cannot be absorbed into the DGLAP-evolved gluon distributions without introducing a steeper $\ln Q^2$ slope of $F_2(x, Q^2)$ than allowed by the HERA data. Therefore, such an enhancement would be a signal of nonlinear effects on the PDF evolution.

The unintegrated ratios, $R(p_T, y, y_2)$, at $|y, y_2| \leq 2$ and $p_T \approx 0$ are quite large for the masses and scales that best agree with the fixed target data. As discussed above, in charm production at central rapidities the PDFs are constrained by the HERA data. For the smaller charm mass and larger scale, $m_c = 1.2$ GeV and $Q^2 = 4m_T^2$, we find $R(p_T, y, y_2) \approx 1.4 - 1.5$. The enhancement is even larger for the smaller Q^2 , $\approx 3.7 - 5.5$ with $m_c = 1.3$ GeV and $Q^2 = m_T^2$. The corresponding enhancement factors are smaller for the upper limit on the charm mass, $m_c = 1.8$ GeV, $1.1 - 1.2$ for $Q^2 = 4m_T^2$ and $1.7 - 2.1$ for $Q^2 = m_T^2$. We have also shown that the enhancement disappears with increasing p_T due to the decreasing importance of the nonlinear terms at larger scales in the PDF Q^2 evolution.

The enhancements of the integrated ratios are somewhat reduced from the unintegrated results above. The rapidity enhancement is $R(y) \approx 1.07 - 1.8$ at midrapidity for the energies studied. For the p_T enhancement, we find $R(p_T = 0) \approx 1.05 - 1.25$ with $Q^2 = 4m_T^2$ and $\approx 1.6 - 4.5$ with $Q^2 = m_T^2$ over the range of m_c we investigate. The mass dependent enhancement, $R(M = 2m_c)$, is similar albeit a bit smaller than $R(p_T = 0)$. At larger p_T and M , the effect dies out rather quickly, see Figs. 4 and 5. The main uncertainty in $R(p_T)$ and $R(M)$ is the sizable contribution from the region $x < 10^{-5}$, currently unconstrained by the HERA data. Thus the enhancement also depends on the extrapolation of the PDFs in this x region.

The enhancement we calculate here should be an upper limit on the possible effect at LO, as we now discuss. The recombination radius of the gluon ladders in the GLRMQ terms was assumed to be the proton radius in the EHKQS analysis [9]. The proton radius was the lower limit on the recombination radius since it gave the strongest possible recombination effect while still describing the H1 data [10] over the full range, $x \geq 3 \times 10^{-5}$ and $Q^2 \geq 1.5$ GeV², without entering the saturation region. In the saturation region, further nonlinear terms become important and the DGLAP+GLRMQ evolution breaks down. Thus, in this approximation, the EHKQS gluon distribution is the upper limit on the LO gluon distribution. The results obtained here are then an upper limit on the enhancement. Studies of the nonlinear PDFs, particularly in the context of NLO DGLAP evolution, are needed to go beyond this approximation.

Finally, we discuss possible detection of this enhancement. Fragmentation and decay should not wipe out the effect, as also seen for shadowing in pA collisions [21]. Although the enhancement $R(p_T, y, y_2)$ is largest, see Figs. 2 and 3, dileptons may not be the best channel to measure the enhancement because the origin of the individual pairs is unknown. The lepton p_T and y also does not correspond directly to the quark p_T and y . In addition, it is not clear how the enhancement survives a minimum p_T cut of the charm decay leptons, even though these decay leptons are a major component of the dilepton spectrum. Further simulations of this would be worthwhile. Since

the enhancement disappears at large p_T , the smallest possible p_T cut is desirable. At higher lepton pair masses, $b\bar{b}$ decays dominate the dilepton mass distributions. The enhancement rapidly decreases with increasing quark mass so that effects on $b\bar{b}$ production are very small.

Single leptons from charm decays [22] may be a better possibility. The single lepton enhancement may, however, be somewhat reduced relative to that of the pair. Of course fully reconstructed D mesons would be the most desirable option. Reconstruction should be possible for $p_T \approx 1$ GeV or less in ALICE with identified kaons [23]. More complete simulations with nonlinear PDFs should thus be performed.

Ideally, a better place to search for the nonlinear effects would be pA collisions at the LHC [24]. The GLRMQ corrections are expected to get an $\propto A^{1/3}$ enhancement from the nuclear size, causing the nonlinearities to be significant at larger values of x and Q^2 than in free protons, see Ref. [25] in Ref. [24]. Thus the enhancement should be more pronounced for nuclei. Before computing charm cross sections in nuclear collisions, however, the nuclear PDFs should be analyzed within the DGLAP+GLRMQ framework, including constraints from nuclear deep inelastic scattering.

Acknowledgments: K.J.E. and V.J.K. gratefully acknowledge the financial support from the Academy of Finland, projects 50338 and 80385. The work of R.V. was supported in part by the Director, Office of Energy Research, Division of Nuclear Physics of the Office of High Energy and Nuclear Physics of the U. S. Department of Energy under Contract Number DE-AC03-76SF00098. Support for R.V.'s visit to Jyväskylä was provided by the Academy of Finland project 50338.

References

- [1] J. Pumplin, D. R. Stump, J. Huston, H. L. Lai, P. Nadolsky and W. K. Tung, JHEP **0207** (2002) 012 [arXiv:hep-ph/0201195].
- [2] D. Stump, J. Huston, J. Pumplin, W. K. Tung, H. L. Lai, S. Kuhlmann and J. F. Owens, arXiv:hep-ph/0303013.
- [3] A. D. Martin, R. G. Roberts, W. J. Stirling and R. S. Thorne, Eur. Phys. J. C **23** (2002) 73 [arXiv:hep-ph/0110215].
- [4] A. D. Martin, R. G. Roberts, W. J. Stirling and R. S. Thorne, Phys. Lett. B **531** (2002) 216 [arXiv:hep-ph/0201127].
- [5] A. D. Martin, R. G. Roberts, W. J. Stirling and R. S. Thorne, arXiv:hep-ph/0308087.
- [6] Y. L. Dokshitzer, Sov. Phys. JETP **46** (1977) 641 [Zh. Eksp. Teor. Fiz. **73** (1977) 1216]; V. N. Gribov and L. N. Lipatov, Yad. Fiz. **15** (1972) 781 [Sov. J. Nucl.

- Phys. **15** (1972) 438]; V. N. Gribov and L. N. Lipatov, Yad. Fiz. **15** (1972) 1218 [Sov. J. Nucl. Phys. **15** (1972) 675]; G. Altarelli and G. Parisi, Nucl. Phys. B **126** (1977) 298.
- [7] L. V. Gribov, E. M. Levin and M. G. Ryskin, Nucl. Phys. B **188** (1981) 555; L. V. Gribov, E. M. Levin and M. G. Ryskin, Phys. Rept. **100** (1983) 1.
 - [8] A. H. Mueller and J. w. Qiu, Nucl. Phys. B **268** (1986) 427.
 - [9] K. J. Eskola, H. Honkanen, V. J. Kolhinen, J. w. Qiu and C. A. Salgado, Nucl. Phys. B **660** (2003) 211 [arXiv:hep-ph/0211239].
 - [10] C. Adloff *et al.* [H1 Collaboration], Eur. Phys. J. C **21** (2001) 33 [arXiv:hep-ex/0012053].
 - [11] R. Vogt, Heavy Ion Phys. **17** (2003) 75 [arXiv:hep-ph/0207359].
 - [12] B. L. Combridge, Nucl. Phys. B **151** (1979) 429.
 - [13] H. L. Lai *et al.* [CTEQ Collaboration], Eur. Phys. J. C **12** (2000) 375 [arXiv:hep-ph/9903282].
 - [14] <http://user.pa.msu.edu/wkt/cteq/cteq6/cteq6pdf.html>
 - [15] A. D. Martin, R. G. Roberts, W. J. Stirling and R. S. Thorne, Eur. Phys. J. C **4** (1998) 463 [arXiv:hep-ph/9803445]; A. D. Martin, R. G. Roberts, W. J. Stirling and R. S. Thorne, Phys. Lett. B **443** (1998) 301 [arXiv:hep-ph/9808371].
 - [16] R. Vogt [Hard Probe Collaboration], Int. J. Mod. Phys. E **12** (2003) 211 [arXiv:hep-ph/0111271].
 - [17] R. Vogt, in proceedings of the 18th *Winter Workshop on Nuclear Dynamics*, edited by R. Bellwied *et al.*, Nassau, The Bahamas, 2002, p. 253.
 - [18] P. Nason, S. Dawson, and R. K. Ellis, Nucl. Phys. **B327** (1989) 49.
 - [19] R. Vogt, Z. Phys. C **71** (1996) 475 [arXiv:hep-ph/9510293].
 - [20] J. C. Collins and R. K. Ellis, Nucl. Phys. B **360** (1991) 3.
 - [21] K. J. Eskola, V. J. Kolhinen and R. Vogt, Nucl. Phys. A **696** (2001) 729 [arXiv:hep-ph/0104124].
 - [22] K. Adcox *et al.* [PHENIX Collaboration], Phys. Rev. Lett. **88** (2002) 192303 [arXiv:nucl-ex/0202002].
 - [23] ALICE Collaboration, Technical Proposal, CERN/LHCC 95-71; ALICE Collaboration, Addendum to the Letter of Intent, CERN/LHCC 95-24; ALICE Collaboration, Addendum to ALICE Proposal, CERN/LHCC 99-13; ALICE Collaboration, Hard Probes in Heavy Ion Collisions at the LHC.

- [24] A. Accardi *et al.*, “Hard probes in heavy ion collisions at the LHC: PDFs, shadowing and pA collisions,” ed. K.J. Eskola, arXiv:hep-ph/0308248.
- [25] K. J. Eskola, H. Honkanen, V. J. Kolhinen, J. w. Qiu and C. A. Salgado, arXiv:hep-ph/0302185.